Polymerization-Induced Phase Separation. 1. Droplet Size Selection Mechanism

Philip K. Chan and Alejandro D. Rey*

Department of Chemical Engineering, McGill University, 3480 University, Montreal, Quebec, H3A 2A7, Canada

Received May 13, 1996; Revised Manuscript Received September 6, 1996[⊗]

ABSTRACT: A model composed of a synthesis of the nonlinear Cahn−Hilliard and Flory−Huggins theories for spinodal decomposition (SD) and a second-order rate equation for the self-condensation of a trifunctional monomer is presented and used to analyze polymerization-induced phase separation (PIPS). The numerical results replicate frequently reported experimental observations on the PIPS of a binary monomer−solvent solution. These observations include a transient periodic concentration spatial profile with a wavelength that decreases with increasing rate constant. In addition, the time evolution of the maximum value of the structure factor exhibits an exponential growth during the early stage, but then slows down in the intermediate stage of SD. Computational analysis shows that, in the PIPS method, the wavelength of the phase-separated structure depends on the complex interaction between the competing polymerization and phase separation processes. The effects of these two competing processes on the characteristic time and length scales of the phase separation phenomena depend on the magnitudes of a scaled diffusion coefficient D for phase separation and a scaled rate constant K_1 for polymerization. As D increases, the dominant dimensionless wavenumber k_m^* also increases, but the phase separation lag time decreases. Similarly, as K_1 increases, k_m^* also increases, but the polymerization lag time decreases. On the basis of these two dimensionless parameters, the dominant wavelength selection mechanism in the PIPS process is identified, which enables the control of morphology during the PIPS phenomena.

1. Introduction

A novel and practical method of producing binary composite materials is by polymerization-induced phase separation (PIPS).[1] It involves polymerizing monomer−solvent solutions so that the system undergoes spinodal decomposition (SD) to form a phase-separated structure (morphology). The PIPS method is more complex than the more common method of thermally induced phase separation (TIPS). In the PIPS method, phase separation and polymerization occur simultaneously. Gunton *et al.*[2] give an extensive review on SD. In addition, SD dynamics in polymer solutions after a thermal quench into the unstable region have been studied numerically by Chan and Rey[3,4] and Jin *et al.*[5] and experimentally by others.[6−9] Moreover, this phenomena have also been extensively studied both numerically[10,11] and experimentally[12,13] in polymer blends.

Doane *et al.*[1] showed that the PIPS method can be used to form a binary composite material called polymer-dispersed liquid crystals (PDLC's). This composite material has great utility as a light shutter, and some examples of applications are switchable windows and billboards. The morphology of PDLC's consists of liquid crystalline droplets dispersed uniformly in a solid polymer matrix. Since the pioneering work of Doane *et al.*,[1] others have also studied experimentally the formation of PDLC's by both the PIPS[14−23] and TIPS[14−16] methods. They studied the phase separation phenomena[14−23] and have shown that PDLC's are formed by SD.[15−18] Moreover, some were also interested in characterizing the electro-optical properties of the thin films that they produced.[1,14,16,19,20,22] The curing temperature does not have to be below the nematic−isotropic transition temperature of the liquid crystal; i.e., the liquid crystal can be isotropic during SD.[14,15,17,18,21] Despite having its formation, morphology, and electro-optical properties well-characterized, the effect of the intimate competitive interactions between the phase separation and polymerization processes on the formation of PDLC's still remains poorly understood. The industrial importance of PDLC films,[24] however, suggests a need to model and simulate the film formation.

Lin and Taylor[25] studied theoretically the PIPS method of producing PDLC's. Their objective was to study the effect of the initial monomer concentration on the characteristic phase separation time. To achieve this, they decoupled the phase separation and polymerization processes, and assumed that phase separation takes place at a well-defined degree of polymerization. The model consists of the Flory−Huggins free energy equation[26,27] to describe phase equilibrium, and a kinetic equation for polymerization that is similar to the one used by Stockmayer.[28] They did not, however, study the concentration spatial profile but alluded to the fact that numerical studies are needed to understand the competing effects of phase separation and polymerization. Recently, Yu *et al.*[29] studied numerically surface effects in PDLC's. Their study, however, considered only the end results of the phase separation process for a fixed solute degree of polymerization. Using a Monte Carlo simulation approach for the PIPS method of forming PDLC's, Jin *et al.*[30] found that the liquid crystalline droplet size can be controlled by the location of the curing point on the binary phase diagram, the polymerization reactivity, or the curing time.

The PIPS method can also be used with other types of polymer systems, such as polymer blends.[31−33] To study the late stages of SD, precursors must be specifically chosen so that gelation does not occur. The scaling results of Kim and Palffy-Muhoray,[17] Chen *et al.*,[32] and Okada *et al.*[33] indicate that there is no universal scaling for the late stage of polymerization-induced SD.

[⊗] Abstract published in *Advance ACS Abstracts,* December 1, 1996.

S0024-9297(96)00690-0 CCC: $12.00

Ohnaga *et al.*[34] studied numerically the phase separation phenomena during continuous quenching. They used the nonlinear Cahn−Hilliard (C-H) equation[2,35,36] and Flory−Huggins (F-H) free energy equation[26,27] to describe the phase separation phenomena. Their objective was to mimic the PIPS process, where the quench depth is continuously increasing with the degree of polymerization. Their model is able to describe qualitatively the morphological development during the PIPS process for several epoxy−polymer mixtures.

Tanaka *et al.*[37] proposed a modified version of the linear C-H equation[2,38] to describe unusual pattern formation under competing phase separation and chemical reaction processes. Their modified equation takes the form of a reaction−diffusion equation, which also incorporates the F-H free energy equation and a first-order rate law for the reaction. Glotzer *et al.*[39] solved numerically a similar reaction−diffusion equation. They found that the chemical reaction can tune the length scale of phase separating patterns.

The objective of this paper is to present results from a numerical study on the isothermal phase separation phenomena during the polymerization of a model binary trifunctional monomer−small molecule solvent solution. This self-condensation polymerization was chosen in the present work because it is simple, yet it still provides the essential physics of network formation. The molecular weight distributions for this case have been fully characterized by Stockmayer[28,40] and Flory.[26,40] It is assumed that, with increasing polymer molecular weight, the phase separation occurs in the unstable region of the binary phase diagram and the solute remains monodisperse. The nonlinear C-H equation and F-H free energy equation are used to describe the phase separation phenomena. The self-condensation polymerization is assumed to follow second-order kinetics. Since we are interested in the effect of the competition between phase separation and polymerization processes on the formation of droplets in PDLC's, the numerical study is restricted to the dynamics of phase-separated structure during the early stage and beginning of the intermediate stage of SD. An emphasis is placed on identifying the mechanisms that control the characteristic time and length scales found in the PIPS process. In a forthcoming paper, which is based on the same primary objective as this one, length scale distribution will be studied.[41] The rest of this paper is organized as follows. The governing equations, auxiliary conditions, and the method of solution are given in section 2. The numerical results are presented, discussed, and contrasted with experimental data in section 3. Finally, conclusions are given in section 4.

2. Problem Formulation and Numerical Methods

2.1. Theory. The nonlinear C-H theory[2,35,36] is based on the following total free energy of an inhomogeneous binary solution:

$$F = \int [f(c) + \kappa(\nabla c)^2] \mathrm{d}V \tag{1}$$

where c is the concentration and κ is a positive parameter related to the interfacial energy constant. In this paper, the concentration (c) is taken to be the solvent volume fraction. The first term on the right hand side of eq 1 is the homogeneous free energy density. The F-H free energy density[26,27] is an appropriate choice for both monomer and polymer solutions. The second term takes into account any increases in free energy due to concentration gradients. Both terms can be obtained from the Taylor series expansion of a free energy density that depends on the concentration and its spatial derivatives.[36] The first term is the zeroth-order term, while the second term is the first nonvanishing correction term of the expansion. The nonlinear C-H equation is derived using the continuity equation, and it is expressed as follows:

$$\frac{\partial c}{\partial t} = \nabla \cdot \left[M \nabla \left[\frac{\partial f(c)}{\partial c} - 2\kappa \nabla^2 c \right] \right] \tag{2}$$

where M is the mobility.

The phase separation phenomena during SD is usually followed experimentally by light, X-ray, or neutron scattering. The scattering pattern consists of a bright ring in a dark background. With time, the brightness intensifies, while the ring radius decreases. Even though this ring is the trademark of SD, numerical results through the structure factor are usually compared to time-resolved scattering intensity profiles.[42]

The F-H free energy density is based on a combinatorial lattice theory and is expressed as follows:[26,27]

$$f(c) = \frac{k_B T}{v} \left[\frac{c}{N_1} \ln c + \frac{(1-c)}{N_2} \ln(1-c) + \chi c(1-c) \right] \tag{3}$$

where k_B is Boltzmann's constant, T is temperature, v is the volume of a cell or segment, c is the solvent volume fraction, and χ is Flory's interaction parameter. N_1 and N_2 are the solvent and solute degrees of polymerization, respectively. For polymer solutions, it is usually assumed that $N_1 = 1$. The interaction parameter is related to T through the following expression:

$$\chi = \frac{1}{2} - \psi \left[1 - \frac{\theta}{T} \right] \tag{4}$$

where ψ is a dimensionless entropy of dilution parameter, θ is the theta temperature, the temperature at which the polymer solution behaves as if it is ideal.[27]

In our numerical study on the thermal-induced SD of polymer solutions, we assumed that the mobility (M) and the parameter related to the interfacial tension (κ) were constants.[3,4] This assumption, however, does not hold in the present study since both M and κ are dependent on the polymer molecular weight (or N_2), which is constantly increasing with time. Moreover, these dependencies can only be approximated for the present complex system, which undergoes cross-linking and network formation. The molecular weight dependence of M can be approximated by applying the Stokes−Einstein equation[43] to a polymer melt. The entanglements of the polymer chains in the melt resemble closely the branching and cross-linking occurring during polymerization considered in this study. Empirical equations are given in the literature relating polymer melt viscosity to the number of backbone atoms.[27,44] The following relation is obtained for the self-condensation of a trifunctional monomer during the early and intermediate stages of SD, where $N_2 < 300$:

$$\mathrm{M} = \frac{M_o}{N_2} \tag{5}$$

The functional dependence of M on N_2 is appropriate

in the present system, since cross-linking hinders molecular movement. The limiting case occurs at gelation ($N_2 \rightarrow \infty$), where the viscosity is infinite and no molecular movement ($M = 0$) is allowed. De Gennes[45] derived an expression for the κ parameter that is appropriate for symmetric polymer blends. The expression contains an enthalpic term that is the product of Flory's interaction parameter (χ) and the square of the effective interaction length between the molecules (l_i^2). It also contains an entropic term that is a function of the Kuhn length and solvent volume fraction (c). For polymer solutions, the length l_i is the radius of gyration (R_g).[46] The enthalpic term is 3 orders of magnitude larger than the entropic term for typical molecular dimensions in polymer solutions.[6] Consequently, the entropic term can be neglected for polymer solutions. Furthermore, for small molecule systems, κ is assumed to be constant; i.e., there is no entropic term as well. Therefore, only the enthalpic term is needed in this study because the binary solution evolves from an initial small molecule system, where $N_1 = N_2 = 1$, to a polymer solution where $N_1 = 1$ but $N_2 > 1$. Even though the solution consists of branch polymer molecules, it is assumed that $l_i = R_g$. Since the radius of gyration is smaller for a nonlinear polymer than for a linear one of the same molecular weight, the following expression is obtained for κ:

$$\kappa = \kappa_o N_2 \tag{6}$$

As the polymer chain grows, so does its interaction with the solvent. This phenomenon is captured in eq 6, since κ is proportional N_2.

The conventional kinetic rate equation for a nth order reaction of a single reactant is expressed as follows:[47]

$$\frac{dp}{dt} = k_1(1 - p)^n \tag{7}$$

where p is the extent of reaction and k_1 is the rate constant. This rate equation is appropriate for the trifunctional monomer A_3 considered in this paper. The monomer undergoes self-condensation to form an infinite network. Since the condensation reaction is bimolecular, $n = 2$. Consequently, the analytical solution to eq 7 for $n = 2$, along with the initial condition $p = 0$, is

$$p = \frac{k_1 t}{1 + k_1 t} \tag{8}$$

Stockmayer[28] and Flory[26] derived the molecular size distribution functions for the self-condensation polymerization of A_3. These distribution functions were then used to obtain the weight average (X_w) and number average (X_n) degrees of polymerization, which are expressed as follow:

$$X_w = \frac{1 + \alpha}{1 - \alpha(f - 1)} \tag{9a}$$

$$X_n = \frac{1}{1 - (\alpha f/2)} \tag{9b}$$

where f is the monomer functionality and α is the branching coefficient. For the single reactant system A_3, $\alpha = p$. In addition, at the gel point, where $\alpha = 0.5$, $X_w \rightarrow \infty$ while $X_n = 4$. Since X_w better reflects the molecular weight growth leading to infinite network formation, it is used in this study to represent the solute degree of polymerization; i.e., $N_2 = X_w$.

2.2. Governing Equations and Auxiliary Conditions. This paper is restricted to a one-dimensional study of the PIPS of a monomer−solvent solution along a line of length L. It is assumed in this study that the speed at which the metastable region crosses the curing point on the phase diagram is sufficiently fast, such that no nuclei can be created during this time interval. Consequently, the isothermal phase separation phenomenon is strictly spinodal decomposition and is governed by the nonlinear C-H and F-H theories given by eqs 2 and 3, respectively. As specified by eq 4, Flory's interaction parameter (χ) is assumed to be a function of temperature only. The polymer molecular weight dependence of the mobility (M) and interfacial parameter (κ) are given by eqs 5 and 6, respectively. In addition, it is assumed that the solvent is a small molecule (i.e., $N_1 = 1$) and the solute is always monodisperse at any degree of polymerization N_2. Hydrodynamic effects are neglected since in concentrated polymer solutions they are only important during the late stage of SD,[6] which is outside of the time range of this study. Furthermore, the self-condensation polymerization of A_3 follows second-order kinetics according to eq 7, while its weight average degree of polymerization (X_w) is described by eq 9a. In this study, the governing equations for phase separation and polymerization are only semicoupled. Equation 7 can be solved analytically and independently of the phase separation process to result in eq 8. However, the governing equation for SD can only be solved numerically if the value of N_2 is known at each time step. This value can be calculated from eqs 8 and 9a for the self-condensation of A_3 for any rate constant (k_1).

The following scaling relations are used to nondimensionalize the governing equations:

$$x^* = \frac{x}{L} \quad \text{(for dimensionless length)}$$

$$T^* = \frac{T}{\theta} \quad \text{(for dimensionless temperature)}$$

$$c^* = c \quad \text{(for dimensionless concentration)}$$

$$t^* = \frac{2M_o\kappa_o t}{L^4} \quad \text{(for dimensionless time)}$$

$$D = \frac{k_B\theta L^2}{2v\kappa_o}\cdot\left(\frac{\text{molecule}}{\text{segments}}\right)^2 \quad \text{(for dimensionless diffusion coefficient)}$$

$$K_1 = \frac{k_1 L^4}{2M_o\kappa_o} \quad \text{(for dimensionless rate constant)}$$

The superscripted asterisks denote dimensionless variables. By incorporating eqs 2, 3, 5, and 6, and using the scaling relations given above, the following dimensionless fourth-order nonlinear partial differential equation is obtained to describe the phase separation process:

$$\frac{\partial c^*}{\partial t^*} = \frac{DT^*}{N_2}\left[-\frac{1}{(c^*)^2} + \frac{1}{N_2}\frac{1}{(1 - c^*)^2}\right]\left[\frac{\partial c^*}{\partial x^*}\right]^2 + \frac{DT^*}{N_2}\left[\frac{1}{c^*} + \frac{1}{N_2}\frac{1}{(1 - c^*)} - 2\chi\right]\left[\frac{\partial^2 c^*}{(\partial x^*)^2}\right] - \frac{\partial^4 c^*}{(\partial x^*)^4} \tag{10}$$

Table 1. Dimensionless Material Parameter Values for Simulation of Polymerization-Induced Spinodal Decomposition

c_o^*	0.6			
T^*	0.6			
χ	1.1667			
ψ	1			
N_1	1			
D	1×10^5	2×10^5	4×10^5	
K_1	5×10^1	5×10^2	2×10^3	4×10^3
	5×10^3	6×10^3	8×10^3	1×10^4
	1.5×10^4	2×10^4	3×10^4	4×10^4
	5×10^4			

An appropriate initial condition for eq 10 is one that captures the concentration fluctuations that are present in a homogeneous binary solution at thermal equilibrium. In addition, two sets of realistic nonperiodic boundary conditions are used in this study. The first set is obtained by noting that there is no mass exchange with the surroundings, while the second set of boundary conditions is obtained by evaluating the functional derivative of F. Expressions for these auxiliary conditions are given in our previous papers.[3,4]

By incorporating eqs 8 and 9a and using the scaling relations given above, the following dimensionless algebraic governing equation is obtained for N_2 ($=X_w$) to describe the polymerization process:

$$N_2 = \frac{1 + 2K_1 t^*}{1 + 2K_1 t^* - fK_1 t^*} \tag{11}$$

In summary, the dependent variables are c^* and N_2, and the independent variables are x^* and t^*. While there is an analytical solution to the partial differential equation describing the polymerization process, there is none for the phase separation process. Therefore, eq 10 and its auxiliary conditions must be solved numerically for $c^*(x^*,t^*)$. The parameters are the dimensionless rate constant (K_1), the dimensionless diffusion coefficient (D), the dimensionless initial average concentration (c_o^*), the dimensionless temperature (T^*), and the interaction parameter (χ). Recall that the interaction parameter (χ) is related to T^* by eq 4, where in this study $\psi = 1$. Although a comprehensive parametric study was performed on D, c_o^*, T^*, and K_1, the limited number of simulation results presented here best reflect the objectives of this paper. The parameter values used in these simulations are given in Table 1. The coordinates (c_o^*, T^*) represent a typical experimental curing point on a binary phase diagram;[1,14,15,17,18] i.e., it is in the one-phase homogeneous region initially, but then it enters and remains in the unstable region at some point during polymerization. In addition, the values for D and K_1 listed in Table 1 are appropriate for a parametric study. At one extreme (low D and K_1), little phase separation occurs, and at the other extreme (high D and K_1), significant phase separation is seen.

Equation 10 and its auxiliary conditions are solved numerically using the same computational method as in our previous papers.[3,4] A linear mesh of 128 nodal points, however, is used in this work.

3. Results and Discussion

Figure 1 is a plot of dimensionless temperature (T^*) versus dimensionless concentration (c^*). It contains the binary phase diagrams for solute degree of polymerizations $N_2 = 1$, 10, and 100. In each case, the solvent degree of polymerization $N_1 = 1$. The solid curves are the binodal lines, and the dashed curves are the spinodal lines. These phase diagrams demonstrate the ubiquitous shift and increasing asymmetry that occurs in the c^*-T^* plane as N_2 increases. The dot at coordinates (0.6, 0.6) represents the curing point, where results will be presented and discussed in this paper. Initially, the solution is composed of a small molecule solvent ($N_1 = 1$) and monomers ($N_2 = 1$). Since the curing point is above the two-phase region, the solution is homogeneous. As N_2 increases, the phase diagram shifts upward and toward higher c^*'s. No phase separation occurs until the curing point is thrust into the unstable region. For the values of c_o^*, T^*, and χ listed in Table 1, this occurs at $N_2 \cong 3.75$ and $\alpha \cong 0.3235$. The value of N_2 is obtained using eq 3. The value of α is then obtained from eq 9a. The time it takes for the spinodal line to cross the initial state is called the dimensionless polymerization lag time (t_o^*). This time is calculated using eq 8; that is,

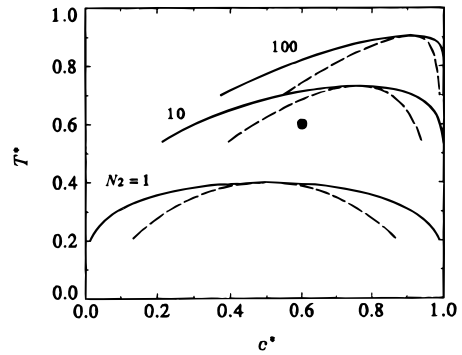

Figure 1. Binary phase diagrams used in this study for $N_1 = 1$ and, from bottom to top, $N_2 = 1$, 10, and 100. They are calculated using Flory−Huggins free energy density with $\psi = 1$. The solid curves are the binodal lines, and the dashed curves are the spinodal lines. The dot at coordinates (0.6, 0.6) represents the curing point. Initially, the system is at $N_1 = N_2 = 1$, and the phase diagram is symmetric. With polymerization, N_2 increases, the phase diagram becomes asymmetric, and the curing point is thrust into the unstable region, where phase separation occurs by spinodal decomposition.

$$t_o^* = \frac{\alpha}{K_1(1 - \alpha)} \tag{12}$$

and then substituting the known values of K_1 and $\alpha = p = 0.3235$. For times $t^* > t_o^*$, the system remains in the unstable region due to the polymerization process. Thus, the process is known as polymerization-induced SD.

Figure 2 shows the concentration spatial profiles $c^*(x^*)$ during the phase separation phenomena for the case of $D = 2 \times 10^5$ and $K_1 = 5 \times 10^4$ at the following dimensionless times: $t^* = 1.21 \times 10^{-5}$ (solid line), $t^* = 1.31 \times 10^{-5}$ (dotted line), and $t^* = 1.47 \times 10^{-5}$ (dashed line). In accordance with the linear C-H theory for SD at early times, the initial random fluctuations develop into a periodic morphology by $t^* = 1.21 \times 10^{-5}$. Regions where $c^* > c_o^*$ ($c^* < c_o^*$) are considered solvent-rich (solute-rich). The third peak at $x^* \cong 0.35$, being relatively small compared to the others, is subsequently absorbed into the two neighboring ones as the system evolves and adjusts to the required wavelength set out by the parameters for this case. While this is happening, the structure remains periodic. It will be shown below that the phase-separating system shown in Figure 2 is in the early stage and beginning of the intermediate stage of SD. Nevertheless, polymerization has no effect

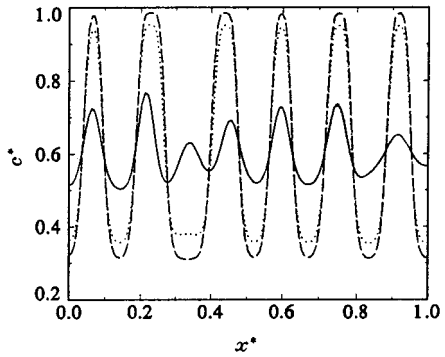

Figure 2. Dimensionless concentration profiles $c^*(x^*)$ formed during the phase separation phenomena for the simulation corresponding to $D = 2 \times 10^5$ and $K_1 = 5 \times 10^4$ at the following dimensionless times: $t^* = 1.21 \times 10^{-5}$ (solid line), $t^* = 1.31 \times 10^{-5}$ (dotted line), and $t^* = 1.47 \times 10^{-5}$ (dashed line). Regions where $c^* > c_o^*$ ($c^* < c_o^*$) are solvent-rich (solute-rich). Since the system is undergoing SD, a periodic morphology forms and evolves.

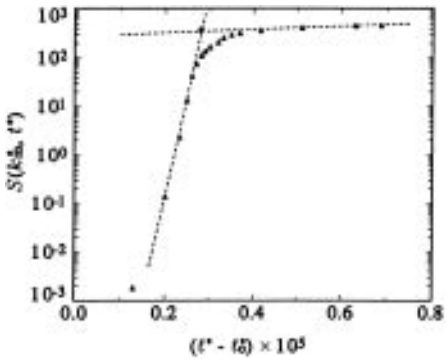

Figure 3. Maximum structure factor $S(k_m^*,t^*)$ as a function of dimensionless time ($t^* - t_o^*$) for the simulation shown in Figure 2. This curve is typical of spinodal decomposition, since there is an exponential growth at first but then it slows down. The dashed lines are tangents along each part of the curve, and their intersection located by the dot gives the transition point between the early and intermediate stages of spinodal decomposition.

on the type of phase-separated structure formed during SD. Yet, it is impossible to determine from these one-dimensional profiles if the morphology is the interconnected structure or the droplet-type morphology observed during SD. However, two-dimensional simulations for the parameters listed in Table 1 show that a droplet-type morphology forms during the PIPS process.[41] This is expected for two reasons. Firstly, the average concentration c_o^* remains an off-critical one at all times during the phase separation phenomena. Secondly, the value of c_o^* used in this paper (see Table 1) is close to the one used in fabricating PDLC's.[1,14,15,17,18] Furthermore, the computations do not converge at $t^* \cong 1.65 \times 10^{-5}$. This problem, typical of phase separation in polymer solutions with highly asymmetric phase diagrams, occurs when c^* at any mesh point approaches unity, as discussed previously by Chan and Rey.[4] This does not, however, prevent the objectives of this paper from being met, since this problem occurs beyond the time range of interest in this paper. It is known and expected that at later times the phase-separated structure coarsens to minimize the interfacial area because of the κ term in eq 1.[3,4]

The dimensionless diffusion coefficient (D) is a ratio of two competing forces; i.e.,

$$D = \frac{\dfrac{k_B \theta L^2}{2v} \cdot \left(\dfrac{\text{molecule}}{\text{segments}}\right)^2}{\kappa_o} \qquad (13)$$

The numerator term is the driving force for phase separation, and the denominator term (κ_o) is the resisting force against phase separation. Thus, as D increases, so does the driving force for phase separation, and a structure of shorter wavelength results. In other words, there is more phase separation. The (molecule/segments) term in eq 13 is squared, while it is not for the dimensionless diffusion coefficient defined for the TIPS process.[3,4] This is due to the fact that the DT^* terms in the governing C-H equation are now divided by N_2, which is introduced into eq 10 by the mobility dependence on the polymer molecular weight. A direct consequence of this point is that to obtain a comparative amount of phase separation, a larger D value is needed in the PIPS process than in the TIPS one. For instance, $D = 2 \times 10^5$ for the PIPS case presented in Figure 2, while $D = 2 \times 10^3$ for a comparative TIPS case.[3]

The time evolution of the concentration spatial profiles shown in Figure 2 is typical of all the cases that were studied. After a characteristic wavenumber (k_m) is chosen at very early times, no additional concentration fluctuations of larger k_m's appear later. This is in contrast to the numerical work of Ohnaga *et al.*,[34] where they found that concentration fluctuations of larger k_m's suddenly appear and superimpose onto existing ones during continuous quenching. As mentioned previously, their goal was to mimic the PIPS process by continuously quenching the sample. This major contrast can be explained by comparing their model with the model presented in this paper. According to the TIPS process, as the quench depth increases, it is expected that larger k_m's appear, since k_m is proportional to the quench depth.[38] Since Ohnaga *et al.*[34] assumed that both M and κ are constant, it is then expected that larger k_m's appear in their work. As shown in section 2.1, this assumption, however, is not sufficiently accurate for binary systems undergoing polymerization. Both M and κ are dependent on the polymer molecular weight, which the model presented here takes into account. As mentioned above, the DT^* terms in the governing equation are divided by N_2. This in effect replaces the driving force for phase separation (i.e., D) by an effective driving force (i.e., D/N_2). Therefore, during polymerization, the effective driving force for phase separation decreases, and a structure of smaller k_m and not a larger one is predicted by the phase separation process. On the other hand, the polymerization process increases the quench depth, which according to the TIPS method, results in increasing k_m^*'s. The transient spatial profiles in Figure 2, therefore, are a result of the complex and intimate interaction between the phase separation and polymerization processes in the PIPS method.

Figure 3 is a semilogarithm plot of the structure factor $S(k_m^*,t^*)$ versus ($t^* - t_o^*$) corresponding to the case shown in Figure 2. $S(k_m^*,t^*)$ is the structure factor $S(k,t)$ evaluated at the dimensionless wavenumber (k_m^*), which is where the maximum of $S(k^*,t^*)$ is located at time t^*. The dashed curves are tangents to each part of the curve, and their intersection, located by the dot, gives the transition point between the early and intermediate stages of SD. The transition point is then the dimensionless transition time (t_t^*) and $S(k_m^*,t_t^*)$, which is the value of $S(k_m^*,t^*)$ at t_t^*. It is noticed that $S(k_m^*,t^*)$, which contains information on both k_m^* and ($c^* - c_o^*$) at t^*, increases exponentially in the early stage but then

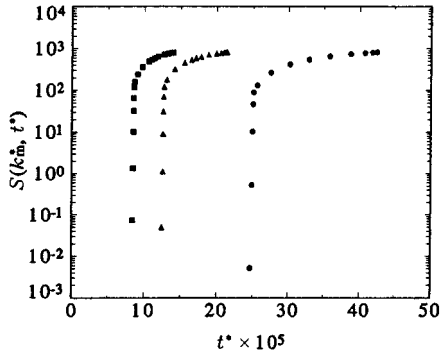

Figure 4. Maximum structure factor $S(k_m^*,t^*)$ as a function of dimensionless time (t^*) for $D = 4 \times 10^5$ and the following dimensionless rate constants: $K_1 = 2000$ (dots), $K_1 = 4000$ (triangles), and $K_1 = 6000$ (squares). Assuming that the phase separation lag time is the same for these three cases, this figure shows that the induction time (or polymerization lag time) decreases as the rate constant increases.

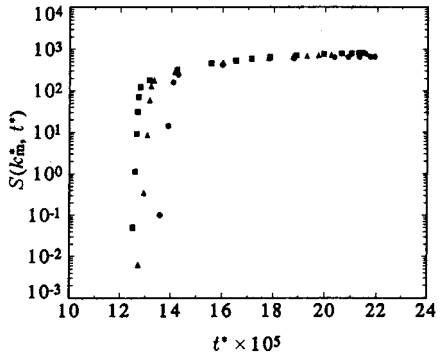

Figure 5. Maximum structure factor $S(k_m^*,t^*)$ as a function of dimensionless time (t^*) for $K_1 = 4000$ and the following dimensionless diffusion coefficients: $D = 1 \times 10^5$ (dots), $D = 2 \times 10^5$ (triangles), and $D = 4 \times 10^5$ (squares). Since the polymerization lag time is the same for these three cases, this figure shows that the induction time (or phase separation lag time) decreases as the dimensionless diffusion coefficient increases.

it saturates as the phase separation enters the intermediate stage. This trend in the time evolution of $S(k_m^*,t^*)$ has already been observed experimentally in PDLC's[17,18] and other polymer systems[31−33] formed by the PIPS process. Consequently, the time range of interest in this paper is the early stage and beginning of the intermediate stage of SD. In addition, the time evolution of $S(k_m^*,t^*)$ during the PIPS process is then similar to that observed in the TIPS process in the time range explored in this study.[4] Moreover, Figure 3 clearly shows that there is indeed a dimensionless induction time ($t_i^* = t_o^* + t_c^*$) since significant phase separation, which is measured by the magnitude of $S(k_m^*,t^*)$, only occurs at $(t^* - t_o^*) > 0$. In addition, since $(t^* - t_o^*) > 0$, there is also a dimensionless phase separation lag time t_c^* that is required for the system to begin phase separation once it has been placed in the unstable region. This lag time is similar to the one identified in the TIPS process.[3]

A parameter that affects the dynamics of phase separation is K_1. Figure 4 shows the structure factor $S(k_m^*,t^*)$ as a function of dimensionless time (t^*) for the following dimensionless rate constants: $K_1 = 2000$ (dots), $K_1 = 4000$ (triangles), and $K_1 = 6000$ (squares). For all three cases, $D = 4 \times 10^5$. In contrast to Figure 3, the abscissa is simply t^*, and not the difference between t^* and t_o^*. This was done so that the effect of K_1 can be easily seen. As K_1 increases, the dimensionless induction time (t_i^*) decreases. It is known that t_c^* is inversely proportional to D.[3] Since D is the same for these three cases, any variations between these three t_c^*'s are negligible. Consequently, it can be concluded that the source for any difference in the dimensionless induction time t_i^* between these three cases is due to the polymerization lag time t_o^*. The trend of t_i^* seen in Figure 4 is explained using eq 12, which states that t_o^* is inversely proportional to K_1. Another observation from this figure is that the beginning of the intermediate stage for all three cases occurs at $S(k_m^*,t^*) \cong 800$. Therefore, their morphological evolution is quite similar in the intermediate stage despite having different dimensionless transition times (t_t^*) between the early and intermediate stages of SD. Since $S(k_m^*,t^*)$ is a complex function of both k_m^* and $(c^* - c_o^*)$, verification can only be made by checking their one-dimensional transient concentration profiles, which was done in this study. The reason for this similarity is that the three K_1's are quite close in magnitude.

Another parameter that affects the dynamics of the phase-separated structure is D. Figure 5 is a plot of $S(k_m^*,t^*)$ versus t^* for the following dimensionless diffusion coefficients: $D = 1 \times 10^5$ (dots), $D = 2 \times 10^5$ (triangles), and $D = 4 \times 10^5$ (squares). For all three cases, $K_1 = 4000$. This means that any variations in t_i^* is due to t_c^*, because t_o^* is the same for these three cases. Figure 5 clearly shows that, as D increases, t_i^* decreases. This relationship reflects the effect which the magnitude of D has in the governing equation. According to eq 10, as D increases, the rate of change of c^* also increases, which means that t_i^* will decrease. This effect is also seen in the TIPS process.[3,4] Another observation can also be made here. Although there is a distinct trend in the order of the three curves at early times, they coincide in the intermediate stage. Their one-dimensional transient concentration profiles show that the phase-separated structures are quite similar. There are, however, differences in the wavelength and amplitude between these three cases. Thus, a plausible reason for this observation is that $S(k_m^*,t^*)$ is a complex function of both k_m^* and $(c^* - c_o^*)$.

As noted in the introduction, the droplet size and distribution are important factors that affect the efficiency of PDLC's as light shutters. In addition, the PIPS process is also used to form other binary composite materials, in which their mechanical properties depend on the droplet size and distribution as well. Therefore, the control of these two factors is crucial during the phase separation phenomena. In this paper, only the control of droplet size is discussed. Droplet size distribution will be studied and discussed in a forthcoming paper.[41]

Simulations were performed on the various combinations of D and K_1 listed in Table 1 at the curing point given in Figure 1. The length d^* is the average dimensionless size of the solvent-rich regions, where $c^* > c_o^*$. In one dimension, d^* is the average dimensionless length of the solvent-rich regions. Moreover, in two dimensions, d^* is the average dimensionless equivalent diameter of the solvent-rich nearly circular regions. Since two-dimensional simulations indicate that the droplet-type morphology forms during the PIPS process for the parameters listed in Table 1,[41] it is assumed that the length d^* presented here represents the average dimensionless droplet diameter.

Figure 6 is a plot of the dimensionless droplet size (d^*) versus the dimensionless rate constant (K_1) for the

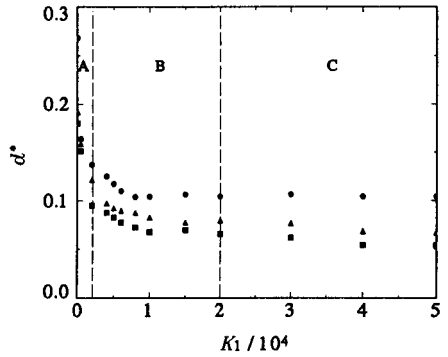

Figure 6. Average dimensionless length of solvent-rich region d^* as a function of dimensionless polymerization rate constant K_1 for the following dimensionless diffusion coefficients: $D = 1 \times 10^5$ (dots), $D = 2 \times 10^5$ (triangles), and $D = 4 \times 10^5$ (squares). The average length d^* is determined by the competition between the polymerization and phase separation processes. Regions A, B, and C denote, respectively, the reaction-controlled regime at low K_1's, the transition regime at intermediate K_1's, and the diffusion-controlled regime at high K_1's.

following dimensionless diffusion coefficients: $D = 1 \times 10^5$ (dots), $D = 2 \times 10^5$ (triangles), and $D = 4 \times 10^5$ (squares). For consistency and to obtain significant phase separation with a regular periodic morphology, the value of d^* is determined at the dimensionless time of $\tau = 1.25 t_t^*$ for all cases listed in Table 1 and shown in Figure 6. In addition, the dimensionless time (τ) is within the time range of interest of this study, and is prior to the time where the aforementioned convergence problem occurs. The value of d^* is then not the droplet size at gelation typically reported in the literature, but rather it is measured at a specific time characteristic to each case. Nevertheless, it does provide practical relative measurements of d^*, which are similar to those observed at gelation.

Three observations can be made from Figure 6. The first observation is that for any K_1 value, d^* decreases as D increases. This relationship between d^* and D has already been observed and discussed previously for the TIPS process.[3,4] The second observation is that for any D value, d^* decreases with increasing K_1, until it reaches a plateau at high K_1 values. This observation is consistent with the Monte Carlo simulation results on the PIPS method of fabricating PDLC's by Jin *et al.*[30] In addition, the fact that d^* is inversely proportional to K_1 has already been seen experimentally in epoxy-based systems[14,21] and in systems undergoing thiol-ene chemistry.[22] The present simulations are in qualitative agreement with these experimental data by making, respectively, the following plausible assumptions: (1) K_1 is proportional to the curing temperature,[14] (2) K_1 is inversely proportional to the cure time constant,[21] and (3) K_1 is proportional to the ultraviolet light intensity.[22] The third observation is that there is a reaction-controlled regime at low K_1 values (region A: $K_1 < 0.2 \times 10^4$), a transition regime at intermediate K_1 values (region B: $0.2 \times 10^4 < K_1 < 2 \times 10^4$), and a diffusion-controlled regime at high K_1 values (region C: $K_1 > 2 \times 10^4$). It is noticed that the crossover dimensionless rate constant between the reaction-controlled and transition regimes ($K_{1,1} \approx 0.2 \times 10^4$) and the crossover dimensionless rate constant between the transition and diffusion-controlled regimes ($K_{1,2} \approx 2 \times 10^4$) are approximately the same for the three D's presented in this figure. A plausible reason for this is that the three D's are quite close in magnitude. The presence of the three

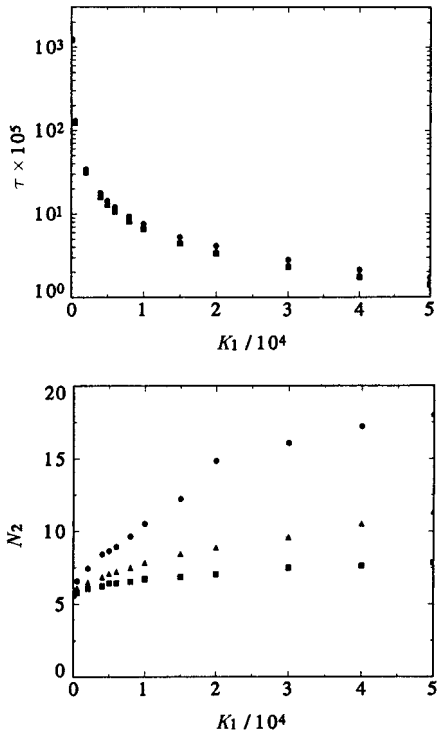

Figure 7. (a) Dimensionless time (τ) and (b) solute degree of polymerization (N_2) as a function of dimensionless rate constant (K_1) for the following dimensionless diffusion coefficients: $D = 1 \times 10^5$ (dots), $D = 2 \times 10^5$ (triangles), and $D = 4 \times 10^5$ (squares).

regimes in Figure 6 can be explained by studying the solute degree of polymerization. Parts a and b of Figure 7 are, respectively, plots of the dimensionless time (τ) and solute degree of polymerization (N_2) versus the dimensionless rate constant (K_1) for the following dimensionless diffusion coefficients: $D = 1 \times 10^5$ (dots), $D = 2 \times 10^5$ (triangles), and $D = 4 \times 10^5$ (squares). Figure 7a shows that the time τ decreases at low K_1 values but eventually reaches a constant value or plateau at high K_1 values as the rate constant increases. This is expected, since eq 12 indicates that the dimensionless polymerization lag time (t_0^*), which is a good indicator of the magnitude of t_t^*, is inversely proportional to K_1. This variation of τ is then reflected in the dependence of N_2 on K_1 through eq 11, and is shown in Figure 7b. In addition, parts a and b of Figure 7a and 7b show, respectively, that in the reaction-controlled regime the time τ and N_2 are invariant with respect to D, but depend on D in the diffusion-controlled regime. According to the linear C-H theory, as N_2 increases, the dominant wavenumber (droplet size) increases (decreases). In other words, $d^* \propto N_2^{-1}$. It must be noted that this proportionality was derived for the TIPS process; however, it can be used as an approximation for the PIPS process. This approximation has already been used successfully by Ohnaga *et al.*[34] in their numerical study of the PIPS process. Therefore, since N_2 is invariant to D (K_1) in the reaction-controlled (diffusion-controlled) regime, it is also expected that d^* to be invariant to D (K_1) in this regime. These results indicate that in the strongly coupled intermediate regime the characteristic droplet size is determined by the complex competition between the polymerization and phase separation processes. This means the droplet size can be controlled through D and K_1.

4. Conclusions

This paper presents results from a one-dimensional numerical study of the PIPS method. The simulations describe the formation of PDLC's by the PIPS method if the curing temperature is above the nematic−isotropic transition temperature. The numerical results from this study replicate frequently reported experimental observations on the formation of PDLC's by the PIPS method. The numerical results indicate that polymerization has no effect on the type of morphology formed during phase separation. A periodic phase-separated structure still forms during spinodal decomposition (SD), as typically observed in TIPS. Two-dimensional simulations were also performed, and their results indicate that a droplet-type morphology forms. This phase-separated structure is consistent with experimental results reported in the literature on the formation of PDLC's by the PIPS method, since the initial concentration is typical of the values used in experiments. The time evolution of the maximum value of the structure factor $S(k_m^*,t^*)$ is also in accordance with experimental results found in the literature on the formation of PDLC's by the PIPS method. The maximum value of the structure factor exhibits an exponential growth during the early stage and then slows down and saturates in the intermediate stage. The polymerization (phase separation) lag time decreases as the dimensionless rate constant (K_1) (dimensionless diffusion coefficient (D)) increases. The dimensionless wavelength, which is twice the dimensionless droplet diameter (d^*), depends on the relative magnitudes of D and K_1. Results from the TIPS method indicate that the droplet diameter decreases with increasing D. On the other hand, during polymerization the quench depth continuously increases since the binary phase diagram constantly rises to higher temperatures. According to the TIPS method, the droplet size decreases with increasing quench depth. Consequently, on the basis of this idea of increasing quench depth during polymerization, the droplet size decreases with increasing polymer molecular weight. The droplet size is then determined by a compromise between these two competing effects. Lastly, the prediction that for a given D the droplet size decreases with increasing K_1 until it reaches a plateau at relatively high K_1's is consistent with reported experimental and numerical results on the PIPS method of forming PDLC's. Three regimes in the d^*-K_1 plane were identified and explained using the fact that $d^* \propto N_2^{-1}$. The results presented in this paper provide a better understanding of the competitive interaction between phase separation and polymerization during the PIPS process. This then allows the droplet size to be controlled to specifications during PDLC film fabrication.

Acknowledgment. This work is supported by a grant from the Natural Sciences and Engineering Research Council of Canada (NSERC). The authors are grateful to CRAY Research (Canada) Inc. for a grant to defray the compuational cost of this work and for technical assistance in using the CRAY C98/8256. P.K.C. acknowledges his postgraduate scholarships from the Natural Sciences and Engineering Research Council of Canada (NSERC) and the Fonds pour la Formation de Chercheurs et l'Aide à la Recherche du Québec (FCAR).

References and Notes

(1) Doane, J. W.; Vaz, N. A.; Wu, B.-G.; Zumer, S. *Appl. Phys. Lett.* **1986**, *48*, 269.
(2) Gunton, J. D.; San Miguel, M.; Sahni, P. S. In *Phase Transitions and Critical Phenomena*; Domb, C., Lebowitz, J. L., Eds.; Academic Press: New York, 1983; Vol. 8.
(3) Chan, P. K.; Rey, A. D. *Comput. Mater. Sci.* **1995**, *3*, 377.
(4) Chan, P. K.; Rey, A. D. *Macromol. Theory Simul.* **1995**, *4*, 873.
(5) Jin, J.-M.; Parbhakar, K.; Dao, L. H. *Comput. Mater. Sci.* **1995**, *4*, 59.
(6) Lal, J.; Bansil, R. *Macromolecules* **1991**, *24*, 290.
(7) Bansil, R. *J. Phys. IV (Paris)* **1993**, *3*, 225.
(8) Kuwahara, N.; Kubota, K. *Phys. Rev. A* **1992**, *45*, 7385.
(9) Kubota, K.; Kuwahara, N. *Mod. Phys. Lett. B* **1992**, *6*, 1089.
(10) Chakrabarti, A.; Toral, R.; Gunton, J. D.; Muthukumar, M. *J. Chem. Phys.* **1990**, *92*, 6899.
(11) Brown, G.; Chakrabarti, A. *Phys. Rev. E* **1993**, *48*, 3705.
(12) Bates, F. S.; Wiltzius, P. *J. Chem. Phys.* **1989**, *91*, 3258.
(13) Hashimoto, T.; Itakura, M.; Hasegawa, H. *J. Chem. Phys.* **1986**, *85*, 6118.
(14) West, J. L. *Mol. Cryst. Liq. Cryst.* **1988**, *157*, 427.
(15) Kyu, T.; Mustafa, M.; Yang, J.-C.; Kim, J. Y.; Palffy-Muhoray, P. *Stud. Polym. Sci.* **1992**, *11*, 245.
(16) Hirai, Y.; Niiyama, S.; Kumai, H.; Gunjima, T. *Proc. SPIE* **1990**, *1257*, 2.
(17) Kim, J. Y.; Palffy-Muhoray, P. *Mol. Cryst. Liq. Cryst.* **1991**, *203*, 93.
(18) Kim, J. Y.; Cho, C. H.; Palffy-Muhoray, P.; Mustafa, M.; Kyu, T. *Phys. Rev. Lett.* **1993**, *71*, 2232.
(19) Vaz, N. A.; Smith, G. W.; Montgomery, G. P. *Mol. Cryst. Liq. Cryst.* **1987**, *146*, 1.
(20) Vaz, N. A.; Smith, G. W.; Montgomery, G. P. *Mol. Cryst. Liq. Cryst.* **1987**, *146*, 17.
(21) Smith, G. W.; Vaz, N. A. *Liq. Cryst.* **1988**, *3*, 543.
(22) Lackner, A. M.; Margerum, J. D.; Ramos, E.; Lim, K.-C. *Proc. SPIE* **1989**, *1080*, 53.
(23) Drzaic, P. S. *Liquid Crystal Dispersions*; World Scientific: Singapore, 1995.
(24) Friedman, A. *Mathematics in Industrial Problems: Part 3*; Springer-Verlag: New York, 1990.
(25) Lin, J.-C.; Taylor, P. L. *Mol. Cryst. Liq. Cryst.* **1993**, *237*, 25.
(26) Flory, P. J. *Principles of Polymer Chemistry*; Cornell University Press: Ithaca, NY, 1953.
(27) Cowie, J. M. G. *Polymers: Chemistry and Physics of Modern Materials*, 2nd ed.; Chapman and Hall: New York, 1991.
(28) Stockmayer, W. H. *J. Chem. Phys.* **1943**, *11*, 45.
(29) Yu, Y.-K.; Wang, X.-Y.; Taylor, P. L. *J. Chem. Phys.* **1996**, *104*, 2725.
(30) Jin, J.-M.; Parbhakar, K.; Dao, L. H. *Liq. Cryst.* **1995**, *19*, 791.
(31) Yamanaka, K.; Inoue, T. *J. Mat. Sci.* **1990**, *25*, 241.
(32) Chen, W.; Kobayashi, S.; Inoue, T.; Ohnaga, T.; Ougizawa, T. *Polymer* **1994**, *35*, 4015.
(33) Okada, M.; Fujimoto, K.; Nose, T. *Macromolecules* **1995**, *28*, 1795.
(34) Ohnaga, T.; Chen, W.; Inoue, T. *Polymer* **1994**, *35*, 3774.
(35) Skripov, V. P.; Skripov, A. V. *Sov. Phys. Usp. (Engl. Transl.)* **1979**, *22*, 389.
(36) Novick-Cohen, A.; Segel, L. A. *Physica D* **1984**, *10*, 277.
(37) Tanaka, H.; Suzuki, T.; Hayashi, T.; Nishi, T. *Macromolecules* **1992**, *25*, 4453.
(38) Cahn, J. W. *J. Chem. Phys.* **1965**, *42*, 93.
(39) Glotzer, S. C.; Di Marzio, E. A.; Muthukumar, M. *Phys. Rev. Lett.* **1995**, *74*, 2034.
(40) Odian, G. *Principles of Polymerization*, 3rd ed.; John Wiley & Sons: New York, 1991.
(41) Chan, P. K.; Rey, A. D. *Macromolecules*, submitted.
(42) Rundman, K. B.; Hilliard, J. E. *Acta Metall.* **1967**, *15*, 1025.
(43) Cussler, E. L. *Diffusion: Mass Transfer in Fluid Systems*; Cambridge University Press: Cambridge, 1984.
(44) Sperling, L. H. *Introduction to Physical Polymer Science*, 2nd ed.; John Wiley and Sons: New York, 1992.
(45) de Gennes, P. G. *J. Chem. Phys.* **1980**, *72*, 4756.
(46) Debye, P. *J. Chem. Phys.* **1959**, *31*, 680.
(47) Barton, J. M. In *Advances in Polymer Science*; Dusek, K., Ed.; Springer-Verlag: New York, 1985; Vol. 72.

MA960690K